Journal of Quantitative Spectroscopy & Radiative Transfer 268 (2021) 107627

Contents lists available at ScienceDirect

Journal of Quantitative Spectroscopy & Radiative Transfer

journal homepage: www.elsevier.com/locate/jqsrt

Characterization of temporal and spatial variability of aerosols from ground-based climatology: towards evaluation of satellite mission requirements

Cheng Chen[a,b,*], Oleg Dubovik[b,*], Gregory L. Schuster[c], David Fuertes[a], Yasjka Meijer[d], Jochen Landgraf[e], Yana Karol[a], Zhengqiang Li[f]

[a] GRASP-SAS, Univ. Lille, Villeneuve d'Ascq, France
[b] Univ. Lille, CNRS, UMR 8518 - LOA - Laboratoire d'Optique Atmosphérique, F-59000 Lille, France
[c] NASA Langley Research Center, Hampton, Virginia, 23681, USA
[d] European Space Agency (ESA), ESTEC, Noordwijk, The Netherlands
[e] SRON Netherlands Institute for Space Research, Utrecht, The Netherlands
[f] Aerospace Information Research Institute, Chinese Academy of Sciences, Beijing, China

ARTICLE INFO

Article history:
Received 10 December 2020
Revised 8 March 2021
Accepted 8 March 2021
Available online 11 March 2021

Keywords:
Aerosol temporal and spatial variability
Spatial resolution
Multi-angular multi-spectral polarimetry
CO2 monitoring mission
Copernicus

ABSTRACT

The high variability of atmospheric aerosol in space and time poses significant challenges for aerosol observation and simulation, as well as for the design of aerosol monitoring systems. Multi-Angular Polarimeters (MAP) have been identified to provide highly accurate data for characterizing in detail columnar properties of atmospheric aerosol. Obtaining such multi-angular observations at high spatial resolution is very challenging, and even more so from satellite observations. At present, the most advanced MAP instruments are intended to provide observations at the spatial resolution of about 2 km to 4 km. The practical understanding of aerosol loading and type variability at fine to moderate spatial scales is still limited. In this paper, we provide insight on the spatial variability of ambient aerosol by combining the full archive of AERONET observations with ancillary wind speeds from the Modern-Era Retrospective Analysis for Research Application, version 2 (MERRA-2) reanalysis dataset. First, the temporal variability of aerosol observations at the smallest AERONET time scale of 15-30 minutes was used to estimate maximum temporal variability of the aerosol loading (aerosol optical depth - AOD), size (Ångström exponent - AE) and absorption (single scattering albedo - SSA) over a selection of 30 typical AERONET sites. In the subsequent step, the derived aerosol temporal variability for AOD, AE and SSA are converted to maximum spatial variability using the mean wind speed from MERRA-2. In the final step, the mean aerosol variability difference was analyzed at spatial scales of 2 km and 4 km, which are the spatial scales considered for the MAP instrument to be deployed as part of the Copernicus Anthropogenic CO_2 Monitoring (CO2M) mission. The mean aerosol parameters obtained at these spatial scales showed very small differences: only 0.004 for AOD (440 nm), 0.004 for AE (440/870), and 0.0005 for SSA (440 nm). The analysis of maximum spatial variation of aerosol concentrations showed some non-negligible spikes, up to ~0.2 for AOD (440 nm) at spatial scales of 4 km. However, those high fluctuations correspond to highly polluted urban sites (i.e. Beijing and Mexico City), and the maximum AOD changes per km remain at ~6% with respect to the total AOD. The maximum spatial variability for AE and SSA also showed no significant deviations at 4 km (<0.2 for AE; <0.03 for SSA). Therefore, we conclude that using a 4 km spatial resolution for MAP sensors is sufficient for capturing the main features of aerosol variability that is required for the CO2M mission.

1. Introduction

The properties of aerosol vary with time and from one location to another, which is due to its short lifetime and various dynamic processes, e.g. transport, advection, deposition, convection

* Corresponding authors.
E-mail addresses: cheng.chen@grasp-sas.com (C. Chen), oleg.dubovik@univ-lille.fr (O. Dubovik).

https://doi.org/10.1016/j.jqsrt.2021.107627

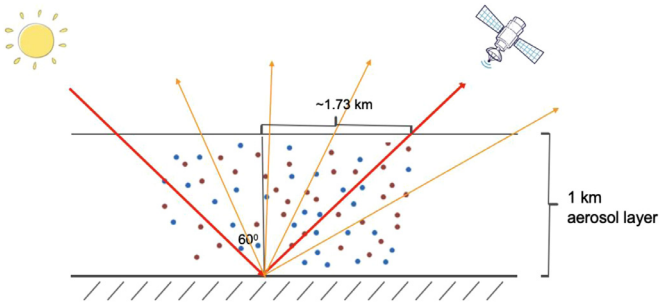

Fig. 1. Schematic overview of multi-angular observations by a satellite instrument. The yellow lines demonstrate the reflected light path for satellite multi-angular observations. The red lines present a typical situation where the solar zenith angle and satellite view zenith angle are 60°, and the aerosol layer height is assumed to be 1 km. Even in this situation where the aerosol layer is quite low, the reflected light is scattered by aerosols in the neighborhood of 1.73 km.

etc. The dynamics of atmospheric aerosol is highly related with local meteorology and their emission sources. The high variability of aerosol poses significant challenges for interpretating aerosol observed by satellite remote sensing and for modeling aerosol transport [1]. Understanding of aerosol temporal and spatial variability is vital for quantifying the climate and health effects of aerosol [2–7], and is also crucial for designing an aerosol observation system. Multi-Angular multi-spectral Polarimetry (MAP) is proven to be suitable solution for aerosol monitoring [8,9]. Furthermore, many MAP sensors are planned to be deployed in the coming few years [9–13]. The understanding of aerosol spatial variability is of particular importance for using the MAP concept for satellite observations, as the multi-angular observations include the observations corresponding to different light paths. As tropospheric aerosol is typically concentrated in elevated layers between 1-5 km, the observations obtained by different angles are affected by aerosol not only directly over the observed spatial sampling area on the ground, but also affected by aerosol in neighboring spatial samples (see Fig. 1). This phenomenon leads to potential inconsistencies of measurements obtained from different geometries (scattering angles) corresponding to the same spatial sample. This is one of the main challenges of multi-angular polarimetry [9]. With this in mind, MAP sensors designed with very high spatial resolution will have a debatable accuracy. Lang et al. [14] discussed the issues of co-registration for the Multi-viewing, Multi-channel and Multi-polarization Imager (3MI), which will be on board of the Metop-SG satellites. They have considered various uncertainties introduced by the inherent differences of the concept in time and the geometry of observations at different angles. Based on the obtained results Lang et al. [14] concluded that, despite the co-registration limitations, the accuracy of 3MI observations remains acceptable at its 4 km spatial measurement resolution.

Many studies have been devoted to large-scale aerosol variability, i.e. inter-continental transport [7,15–17], inter-annual trends [18–23], seasonal and monthly climatologies [24,25], and mesoscale variations [26]. In the air quality community, the spatial resolution of satellite AOD is crucial for prediction of the surface particle matter (PM) concentration, since many studies indicate a tendency for satellite AOD products generated at higher spatial resolutions to provide better AOD-PM relationships over urban areas [27–30]. Several studies have investigated the AOD spatial variability of satellite products ([31,32]), but the results were limited by the product resolution; for example, many of the widely used MODIS Dark Target and Deep Blue products have a spatial resolution of 10 km at nadir [33,34], and the latest products have a 3 km resolution [35]. The MODIS MAIAC products retrieve AOD at 1 km spatial resolution [36], which offers opportunities to analyze AOD variability at a resolution that is considered to be promising for the air quality community ([27–30,37,38]). However, even 1 km resolution satellite AODs are affected by surrounding pixels, since the light path reaching the satellite sensor must pass through more than a single 1-km column (see Fig. 1). Additionally, the reflected radiation measured by orbital instruments is strongly affected by multiple scattering, and this scattering likely includes an atmospheric domain that exceeds a 1 km column. Also, the separation of aerosol and reflectance is rather challenging from single-viewing satellite observations (e.g., MODIS), especially over heterogeneous land surfaces. Also, MAIAC retrievals rely on some a priori spatial and temporal constrains [36]. Therefore, the derived AOD values over 1 km pixel are not completely independent with the values over other surrounding pixels and may be affected by assumptions. Moreover, the commonly used polar-orbiting satellite products provide rather coarse time sampling, typically with a revisit time of 1-2 days per spatial sample and limited to clear sky conditions, which further limits the temporal revisit time. Therefore, analyzing temporal variability of aerosol even using advanced satellite products involves several challenges that do not present in direct Sun ground-based observations.

Indeed, ground-based measurements such as the Aerosol Robotic Network (AERONET) [39] affected by much fewer uncertain factors and, therefore AERONET AOD products are more robust comparing to those from satellite measurements and provide aerosol observations with substantially higher temporal resolution. Although AERONET observations are “point measurements” obtained over fixed sites, the temporal records with 15 min resolution is a solid base for analyzing spatial variability once combined with the aerosol data with ancillary meteorological data. For example, Smirnov et al. [40] used the surface wind speed to analyse the spatial variability of columar aerosol optical properties at the Midway Island AERONET site. The results of these studies suggested a significant correlation between aerosol optical depth (AOD or τ) and wind speed as well as an anticorrelation between Ångström Exponent (AE or α) and wind speed. Additionally, Kinne et al. [41] used AERONET data to evaluate satellite products at mesoscale spatial ranges. Specifically, they assigned ranges and other quality scores for multiple AERONET sites to calculate their representativeness at the mesoscale spatial ranges of 100, 300, 500 or 900 km. However, the ranges and adopted quality scores were based upon a priori operational knowledge and experience of each site.

The objective of this study is to evaluate the spatial variability of aerosols at the scales typical for the observations required to support the Copernicus Anthropogeneic CO_2 Monitoring (CO2M) mission. Specifically, we focus on evaluating differences in spatial variability between 2 km and 4 km spatial resolution considered for the MAP instrument [11,42]. As such, the explicit objective of this study is to determine whether characterizing aerosol with a MAP at a spatial resolution of 4 km is sufficient for the CO2M mission. We aim to derive the mean aerosol varibility at 2 km and 4 km and to evaluate possible differences in aerosol characterization. The analysis relies on the comprehensive dataset and frequent aerosol measurments collected during more than 30 years by AERONET ground-based measurements [39]. Specifically, we intend to convert the estimates of temporal aerosol variablity to estimates of spatial variability by using ancillary data from the Modern-Era Retrospective Analysis for Research Application, version 2 (MERRA-2) reanalysis [43].

Table 1
List of AERONET sites used in this study. The site ID, site name, location, typical aerosol type, mean AOD at 440 nm ($\overline{\tau_{440}}$), mean AE (440/870) ($\overline{\alpha_{440/870}}$), starting date for data collection, as well as number of observations for each site are shown in the table. The 1σ in the brackets for $\overline{\tau_{440}}$ and $\overline{\alpha_{440/870}}$ are standard deviation of the mean values.

# ID	Site Name	Location	Type	$\bar{\tau}_{440}$ (1σ)	$\bar{\alpha}_{440/870}$ (1σ)	Start Date	N Obs.
1	GSFC	North America	Urban	0.21 (0.21)	1.61 (0.32)	1993.05	187, 382
2	Mexico_City	North America	Urban	0.38 (0.27)	1.58 (0.31)	1999.02	74, 161
3	Guadeloup	Centre America	Dust	0.15 (0.14)	0.35 (0.39)	1997.02	45, 294
4	Alta_Floresta	South America	Biomass burning	0.42 (0.65)	1.39 (0.44)	1993.06	84, 020
5	Arica	South America	Urban	0.25 (0.12)	1.07 (0.23)	1998.05	105, 100
6	CUIABA-MIRANDA	South America	Biomass burning	0.32 (0.48)	1.34 (0.39)	2001.03	66, 681
7	Banizoumbou	Africa	Dust	0.46 (0.33)	0.35 (0.25)	1995.10	181, 836
8	Capo_Verde	Africa	Dust	0.34 (0.26)	0.28 (0.23)	1994.10	97, 458
9	Dakar	Africa	Dust/BB	0.44 (0.28)	0.35 (0.24)	1996.12	169, 199
10	Ilorin	Africa	Dust/BB	0.80 (0.48)	0.66 (0.32)	1998.04	100, 815
11	Mongu	Africa	Biomass burning	0.34 (0.30)	1.70 (0.34)	1995.06	110, 302
12	Santa_Cruz_Tenerife	Africa	Coastal	0.18 (0.18)	0.58 (0.36)	2004.07	158, 225
13	REUNION_ST_DENIS	Africa	Coastal	0.08 (0.05)	0.72 (0.40)	1997.06	85, 645
14	FORTH_CRETE	Europe	Coastal/Urban	0.21 (0.11)	1.15 (0.50)	2003.01	82, 167
15	Granada	Europe	Urban	0.16 (0.10)	1.11 (0.45)	2004.12	151, 660
16	Lille	Europe	Urban	0.22 (0.17)	1.29 (0.41)	1994.11	88, 864
17	Moscow_MSU_MO	Europe	Urban	0.24 (0.25)	1.43 (0.31)	2001.08	69, 277
18	Rome_Tor_Vergata	Europe	Urban	0.21 (0.13)	1.32 (0.41)	2001.02	127, 681
19	Thessaloniki	Europe	Urban	0.27 (0.16)	1.56 (0.36)	2003.06	104, 444
20	Beijing	East Asia	Urban/Dust	0.67 (0.71)	1.12 (0.31)	2001.03	107, 885
21	Shirahama	East Asia	Coastal	0.29 (0.20)	1.24 (0.36)	2000.10	111, 010
22	XiangHe	East Asia	Urban/Dust	0.70 (0.72)	1.16 (0.31)	2001.03	139, 280
23	Kanpur	Central Asia	Urban/Dust	0.72 (0.36)	0.99 (0.40)	2001.01	159, 907
24	Silpakorn_Univ	Central Asia	Biomass burning	0.57 (0.37)	1.39 (0.34)	2006.08	118, 425
25	Singapore	Central Asia	Urban/BB	0.51 (0.61)	1.39 (0.32)	2006.11	50, 348
26	IMS-METU-ERDEMLI	West Asia	Coastal/Urban	0.29 (0.17)	1.28 (0.36)	1999.11	112, 828
27	SEDE_BOKER	West Asia	Dust	0.20 (0.13)	0.93 (0.45)	1995.03	259, 871
28	Solar_Village	West Asia	Dust	0.35 (0.21)	0.54 (0.34)	1999.02	182, 322
29	Lake_Argyle	Oceania	Biomass burning	0.14 (0.14)	1.11 (0.45)	2001.10	151, 023
30	Lanai	Oceania	Coastal	0.08 (0.06)	0.52 (0.43)	1996.08	46, 172

2. Data description

2.1. AERONET aerosol dataset

AERONET is a global distributed network of well-calibrated sun photometers [39]. By measuring sun direct radiances, AERONET provides high temporal (every ∼15 minutes in daytime) multi-wavelength AOD products with high accuracy (±0.01∼0.02). In addition, almucantar measurements of sky radiances can be converted by an inversion algorithm [44–46] to retrieve aerosol microphysical properties, e.g. aerosol size distribution, complex refractive index, particle sphericity, aerosol single scattering albedo (SSA or ω), etc. [2]. Generally, the accuracy of AERONET inversion products is related to the total aerosol loading. The SSA accuracy is estimated to be ±0.03 when AOD (440 nm) is higher than 0.2, and ±0.05-0.07 when AOD is lower than 0.2 [45].

In this study, we selected 30 AERONET sites, which represent very different aerosol conditions to best represent the aerosol temporal and spatial variability. Any of the 30 sites has at least 40, 000 direct Sun AOD measurements and has been operational for more than 10 years. Detailed information of these sites is listed in Table 1, and their geo-location is shown as white circles on a global map in Fig. 2. We use AERONET Version 3 Level 1.5 (Last access: 2019-07-05) [47] data in our analysis. In order to ensure the quliaty of inversion products, we further select the data satisfying the requirements for Level 2.0 but relax the AOD limits by using the flag 'If_Retrieval_is_L2(without_L2_0.4_AOD_440_threshold)'. This option indicates the satisfication for Level 2 requirements (i.e. post-calibration, cloud-mask etc.) except for 0.4 threshold of AOD 440 nm, which selects high quality inversion products as much as possible while including low AOD conditions. We focus on three main parameters: (i) AOD; (ii) Ångström Exponent (AE) and (iii) SSA, which represent aerosol terms of its loading, size distribution and absorbing properties, respectively.

2.2. MERRA-2 reanalysis wind speed

The newly released MERRA-2 [43] is a global earth system model based reanalysis dataset with data assimilation. MERRA-2 provides long-term (1980 - onwards) reanalysis dataset of climate system. In this study, we will use MERRA-2 10-m wind speed data (Last access: 2019-04-23) as ancillary data to access the aerosol temporal and spatial variability. The evaluation of MERRA-2 wind speed dataset indicates a clear improvement to its predecessor (MERRA), which tended to underestimate winds over ocean and overestimate winds over land. The errors for both MERRA and MERRA-2 are relatively higher at coastal and land areas than in open ocean [48]. Fig. 2 shows the global mean (2000-2018) 10-m wind speed and direction climatology from MERRA-2 dataset.

Fig. 3 shows the scatter plots of mean AOD (440 nm) versus mean AE (440/870 nm) and the mean 10-m wind speed for all 30 AERONET sites. Evidently, the high wind speed is mainly associated with low AOD and large particles (small AE). Hence, there is a demand to investigate the wind speed related aerosol temporal and spatial variability.

3. Method

3.1. Estimation of aerosol temporal variability

In order to study aerosol variability, we have used the most frequent AOD AERONET observations. The AOD (τ) and AE (α) observations obtained at each ∼15 min were used to evaluate aerosol variability within each time window relying on linear interpolation. The obtained slopes of aerosol variability in time were inter-

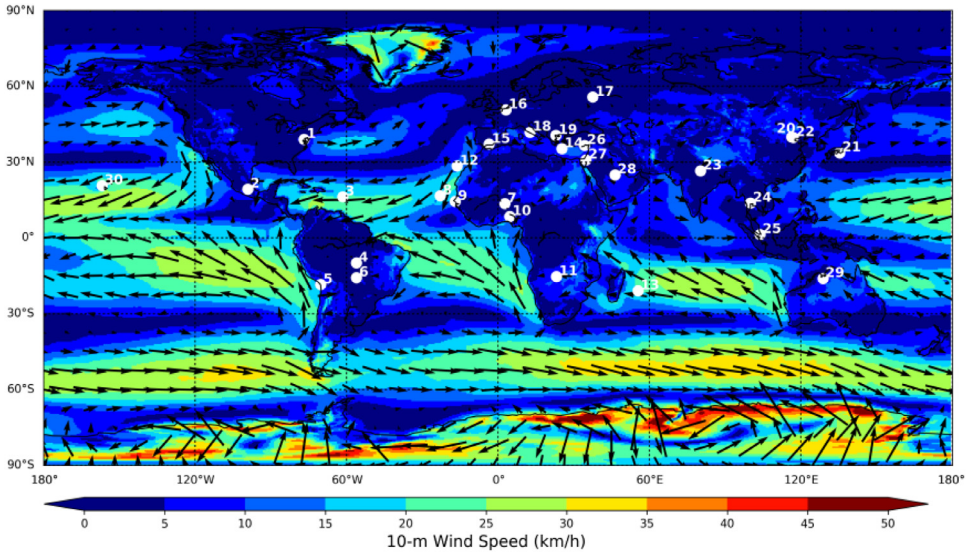

Fig. 2. Global mean 10-m wind speed and direction from MERRA-2 reanalysis (2000-2018). The geo-location of 30 AERONET sites are also shown as white circle, and the site numbers are corresponding to #ID in Table 1.

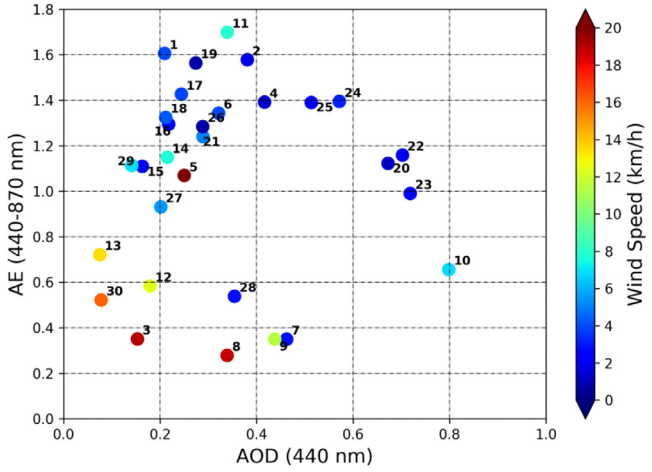

Fig. 3. Scatter plots of mean AOD (440 nm) vs. mean AE (440/870 nm) for all 30 sites. The color represents mean 10-m wind speed of this site for the data-collecting period. The site number (corresponding to the #ID in Table 1) is present close to each circle.

preted as characteristics of aerosol temporal variability. The information about aerosol SSA (ω) is provided by AERONET using sky-scanning diffuse radiances observations [44] that are obtained less frequently than direct Sun measurements, with the interval of ~0.5 hour [39,49]. Correspondingly, the time windows of 0.5, 1.0, 1.5, 2.0, 3.0, 3.5 and 4.0 hour were used for analysis of aerosol (AOD, AE and SSA) variability.

We use the AERONET dataset to calculate the maximum temporal variability of AOD, AE, and SSA. We adopt 8 time windows of Δt_i= 0.5, 1.0, 1.5, 2.0, 2.5, 3.0, 3.5 and 4.0 hour. All available measurements at a site are fragmented according to these time windows, and the maximum absolute aerosol variability of each time fragment are averaged for all available data at a specific site. So for example, the mean of the maximum absolute temporal variability (MMAV) of AOD (τ) during time window Δt_i can be expressed mathematically as $\mathrm{MMAV}_\tau(\Delta t_i) = \overline{(|\tau_\lambda(t+\Delta t_i) - \tau_\lambda(t)|_{\max})}$. Next, we define the temporal variability of τ_λ as the slope of $\mathrm{MMAV}_\tau(\Delta t_i)$ vs. Δt_i, which we call $\mathrm{TV}_{\mathrm{AOD}}$. We use AERONET data to obtain this slope from the following linear regression:

$$\begin{aligned}\mathrm{MMAV}_\tau(\Delta t_i) &= \overline{(|\tau_\lambda(t+\Delta t_i) - \tau_\lambda(t)|_{\max})} \\ &= \mathrm{TV}_{\mathrm{AOD}}(\lambda) \times \Delta t_i + \beta_\tau(\lambda),\end{aligned} \quad (1)$$

Likewise, the AE (α) and SSA (ω) temporal variabilities $\mathrm{TV}_{\mathrm{AE}}$ and $\mathrm{TV}_{\mathrm{SSA}}$ are estimated using the corresponding regressions:

$$\mathrm{MMAV}_\alpha(\Delta t_i) = \overline{(|\alpha(t+\Delta t_i) - \alpha(t)|_{\max})} = \mathrm{TV}_{\mathrm{AE}} \times \Delta t_i + \beta_\alpha, \quad (2)$$

and

$$\begin{aligned}\mathrm{MMAV}_\omega(\Delta t_i) &= \overline{(|\omega_\lambda(t+\Delta t_i) - \omega_\lambda(t)|_{\max})} \\ &= \mathrm{TV}_{\mathrm{SSA}}(\lambda) \times \Delta t_i + \beta_\omega(\lambda),\end{aligned} \quad (3)$$

where λ denotes the wavelength; t reprensents time for each individual measurement. We found that the significance level of the derived $\mathrm{TV}_{\mathrm{AOD}}(\lambda)$, $\mathrm{TV}_{\mathrm{AE}}$ and $\mathrm{TV}_{\mathrm{SSA}}(\lambda)$ are always greater than 99% (i.e. p-values are less than 0.01). The units for $\mathrm{TV}_{\mathrm{AOD}}(\lambda)$, $\mathrm{TV}_{\mathrm{AE}}$ and $\mathrm{TV}_{\mathrm{SSA}}(\lambda)$ are ΔAOD/hour, ΔAE/hour and ΔSSA/hour respectively.

Fig. 4 shows the estimation of aerosol temporal variability over the AERONET sites Alta_Floresta (# 4) and Beijing (# 20) for spectral AOD (at 440, 675, 870 and 1020 nm), AE (440/870) and spectral SSA (at 440, 675, 870 and 1020 nm). The circles represent the mean of the maximum absolute temporal variabilities for AOD, AE and SSA for each Δt_i. The number of data points used for calculating the mean at each Δt_i is presented by the crosses and right axis. The dotted line indicates the linear fit of these time dependent means of maximum variabilities, and the slopes of the linear fit can be interpreted as temporal variability ($\mathrm{TV}_{\mathrm{AOD}}(\lambda)$, $\mathrm{TV}_{\mathrm{AE}}$ and $\mathrm{TV}_{\mathrm{SSA}}(\lambda)$). $\mathrm{TV}_{\mathrm{AOD}}$(440 nm) indicates the AOD (440 nm) temporal variability, which is 0.024 per hour (/h) over Alta_Floresta (# 4) and 0.047/h over Beijing (# 20) respectively. By taking into account the mean AOD (440 nm) of 0.42 (Alta_Floresta) and 0.67 (Beijing) respectively, the relative AOD variability in an hour are ~6%-7%. The $\mathrm{TV}_{\mathrm{AE}}$ (440/870) over Alta_Floresta (# 4) and Beijing (# 20) are 0.048/h and 0.031/h respectively, which account for ~3% of the mean AE. At the same time, the absolute values of the spectral $\mathrm{TV}_{\mathrm{SSA}}(\lambda)$ over these 2 sites is low, ~0.004-0.006. In general, the aerosol loading, i.e. AOD, varies more than the parameters for aerosol size (AE) and absorption (SSA). It should be noted that the direct Sun data of AOD and AE are much more frequent than the SSA. The number of AOD and AE time windows decreases

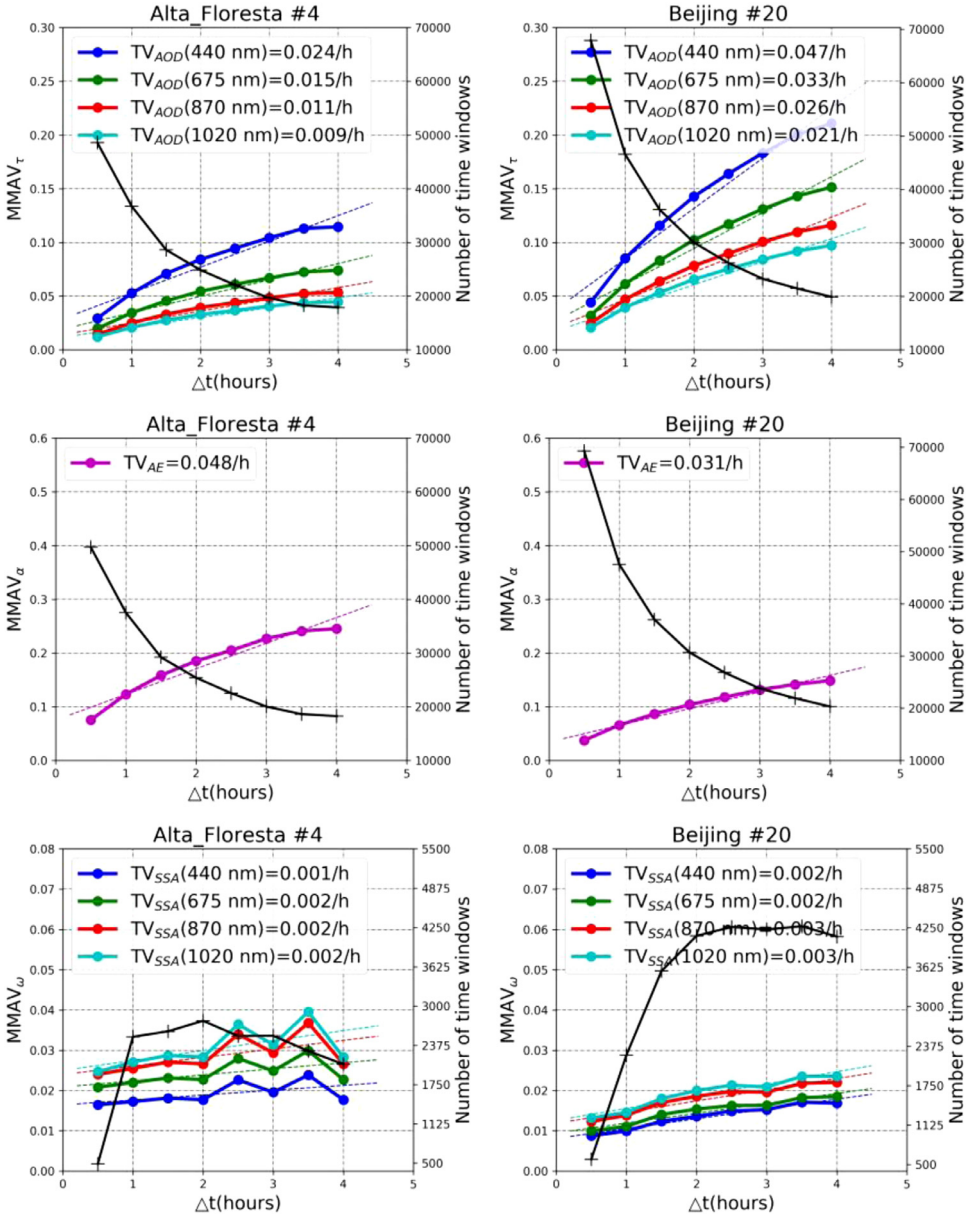

Fig. 4. $TV_{AOD}(\lambda)$, TV_{AE} and $TV_{SSA}(\lambda)$ estimation over Alta_Floresta (site ID # 4, left column) and Beijing (site ID # 20, right column). The circles represent the mean of the $MMAV_\tau$, $MMAV_\alpha$ and $MMAV_\omega$ (top to bottom, respectively) for each time window Δt_i. The number of data points used for calculating the MMAV at each $\Delta t_i$is presenedt by crosses and right axis. The dotted line indicates the linear fit of these time dependent MMAV, and the slopes of the linear fit can be interpreted as the temporal variabilities ($TV_{AOD}(\lambda)$, TV_{AE} and $TV_{SSA}(\lambda)$).

with the increasing of Δt_i. While for SSA the number of time windows rapidly increases going from $\Delta t_i = 0.5h$ to $\Delta t_i = 2h$, where it reaches its maximum and then even sligthly decreases going to $\Delta t_i = 4h$. This is due to a consequence of the sky-scanning Almucantar measurements which are carried out hourly from 9:00 to 15:00 local time or optical air mass equals to 4, 3, 2, and 1.7 both in the morning and the afternoon.

3.2. Estimation of aerosol spatial variability

We base our aerosol spatial variability estimation over each AERONET site on the aerosol temporal variability (see Section 3.1) and the mean wind speed $\bar{v}$ (unit: km/h), which is adopted from MERRA-2 reanalysis (2000-2018) (see Fig. 2). The AOD spatial variability (SV_{AOD}, with as unit ΔAOD/km), the AE spatial variability (SV_{AE}, with as unit ΔAE/km) and the SSA spatial variability (SV_{SSA}, with as unit ΔSSA/km) are estimated based on the following equations:

$$SV_{AOD}(\lambda) = TV_{AOD}(\lambda)/\bar{v} \tag{4}$$

$$SV_{AE} = TV_{AE}/\bar{v} \tag{5}$$

$$SV_{SSA}(\lambda) = TV_{SSA}(\lambda)/\bar{v} \tag{6}$$

Thus, aerosol spatial variability is linked with the derived temporal variability using wind speed in Eqs. (4–6); here, we assume that the spatial variability changes gradually with distance in the downwind direction. Note that Eqs. (4–6) also indicate that high aerosol temporal variability and low wind speed correspond to high aerosol spatial variabilities.

3.3. Estimation of aerosol mean variability difference in 2 km and 4 km grid boxes

The typical spatial resolution under consideration for the next generation multi-angular polarimeter is 2 to 4 km. Therefore, we need to evaluate the aerosol spatial variability difference at these scales and identify possible important differences in aerosol characterization associated with such grid box sizes. Here, the mean spatial variability differences ($MSVD_{AOD}$, $MSVD_{AE}$ and $MSVD_{SSA}$) are estimated by the conversion of the targeted spatial resolution (d_i) to a time window:

$$\delta t_i = \frac{d_i}{\bar{v}},\ \{d_i = 2\ or\ 4\ \text{km}\} \tag{7}$$

where d_i is the distance in kilometer (e.g. 2 km and 4 km) and $\bar{v}$ is the mean wind speed (unit: km/h). The δt_i is the time window with respect to the corresponding distance, and δt_i differs from site to site. A higher mean wind speed at a site corresponds to a smaller time window. Then the mean spatial variability differences are estimated as follows:

$$\mathrm{MSVD}_{\mathrm{AOD}}(\lambda) = \left\langle \overline{\tau_\lambda(t+\delta t_{4\mathrm{km}})} - \overline{\tau_\lambda(t+\delta t_{2\mathrm{km}})} \right\rangle, \tag{8}$$

$$\mathrm{MSVD}_{\mathrm{AE}} = \left\langle \overline{\alpha(t+\delta t_{4\mathrm{km}})} - \overline{\alpha(t+\delta t_{2\mathrm{km}})} \right\rangle, \tag{9}$$

$$\mathrm{MSVD}_{\mathrm{SSA}}(\lambda) = \left\langle \overline{\omega_\lambda(t+\delta t_{4\mathrm{km}})} - \overline{\omega_\lambda(t+\delta t_{2\mathrm{km}})} \right\rangle, \tag{10}$$

where $\overline{\tau_\lambda(t+\delta t_{4\mathrm{km}})}$ and $\overline{\tau_\lambda(t+\delta t_{2\mathrm{km}})}$ are the mean AOD at 4 km and 2 km; $\overline{\alpha(t+\delta t_{4\mathrm{km}})}$ and $\overline{\alpha(t+\delta t_{2\mathrm{km}})}$ are the mean AE at 4 km and 2 km; and $\overline{\omega_\lambda(t+\delta t_{4\mathrm{km}})}$ and $\overline{\omega_\lambda(t+\delta t_{2\mathrm{km}})}$ represents the mean SSA at 4 km and 2 km, respectively. Note that the mean variability of 2 km and 4 km windows are used here, which is different from the temporal and spatial variability as estimated in Sections 3.1 and 3.2, where the maximum variability was derived.

4. Results and discussions

Based on the approach described in Section 3, we can now estimate the aerosol temporal variability, the maximum aerosol spatial variability and the mean aerosol spatial variability difference at 2 km and 4 km sized grid boxes for the full archive of AERONET sites, as listed in Table 1.

4.1. Aerosol temporal variability

The results for TV_{AOD} and TV_{SSA} were derived for all 30 AERONET sites at four wavelengths: 440, 675, 870 and 1020 nm. The values of TV_{AE} were estimated using the AOD at two wavelengths: 440 and 870 nm. We already presented the results for Alta_Floresta and Beijing in Fig. 4 of Section 3. We selected these sites because their aerosol temporal variability (ΔAOD/h and ΔAE/h) is among the highest of all AERONET sites. The TV_{AOD} has significantly higher values at the 440 nm wavelength. Therefore, the following illustrations will be focused on TV_{AOD}(440 nm). While the TV_{SSA} values are generally higher at the longest wavelength 1020 nm, the TV_{SSA} varies only slightly with wavelength by about 0.001-0.002 per hour, which is very small. Therefore, the illustrations of TV_{SSA} are also provided at 440 nm for consistency with the TV_{AOD}.

The mean TV_{AOD}(440 nm) for the 30 sites is ~0.018 per hour (1σ=0.011). Fig. 5a shows the AOD temporal variability at 440 nm over all considered AERONET sites. The site numbers correspond to the #ID in Table 1. The AOD temporal variability TV_{AOD} (ΔAOD/hour) is relatively high over urban sites (e.g. #2-Mexico_City, #20-Beijing and #22-Xianghe), while TV_{AOD} is low over oceanic sites (e.g. #13-REUNION_ST_DENIS and #30-Lanai). The highest value is ~0.047/h over Beijing and the lowest value is ~0.005/h over REUNION_ST_DENIS. Conclusions like these are as expected and logical since Beijing has one of the highest mean AOD values, while REUNION_ST_DENIS on the other hand is the cleanest AERONET site with the lowest mean AOD (see Table 1).

The AE (440/870) temporal variability (TV_{AE}) over the 30 AERONET sites is presented in Fig. 5b. The mean TV_{AE} over all sites is 0.034 per hour (1σ=0.010). Relatively low values are observed over sites #8 Capo Verde (~0.014/h), #7 Banizoumbou (0.016/h) and #9 Dakar (~0.017/h). The highest TV_{AE} (~0.051/h) is observed at the island site #30 Lanai, which is expected to be a result of the high mean wind speed that causing an influx of large sea salt particles [40].

Fig. 5c presents the TV_{SSA}(440 nm) over the 30 AERONET sites. All the sites show low variability, as all the values are close or even within the AERONET Level 2 standard accuracy of ~0.03. The mean TV_{SSA}(440 nm) is 0.003/h (1σ=0.002). The maximum value of ~0.008/h is observed over the site #29 Lake Argyle, which is geneally affected by biomass buring.

4.2. Aerosol spatial variability

As presented in Section 3, in this study we estimated the aerosol spatial variability from the aerosol temporal variability using mean wind speed. This section shows the results of SV_{AOD} (ΔAOD/km), SV_{AE} (ΔAE/km) and SV_{SSA} (ΔSSA/km), which can provide important information on aerosol spatial variability as needed for optimizing the design of MAP sensors.

The mean SV_{AOD}(440 nm) is estimated at 0.008 per km (1σ=0.009). The AOD spatial variability over the 30 AERONET sites is shown in Fig. 6a. High AOD spatial variability is observed mainly over urban sites (e.g. #20 Beijing ~0.036/km, #22 Xianghe ~0.023/km, #2 Mexico City ~0.023/km, #26 IMS-METU-ERDEMLI ~0.023/km and #19 Thessaloniki ~0.020/km). Low spatial variability can be found over costal oceanic sites (e.g. #3 Guadeloup ~0.0003/km and #30 Lanai ~0.0003/km), which suggests that aerosol is there more homogeneous than in other regions. Correspondingly, the AOD (440 nm) variability at a 4 km scale (by a factor of 4 to SV_{AOD}) is ~0.032 (the mean over 30 AERONET sites), which is of the same order of magnitude as the AERONET AOD uncertainty (±0.01-0.02). Nevertheless, over regions with high aerosol loading, the AOD (440 nm) variability at 4 km scale can reach values of ~0.1-0.15, which represent for ~10-20% of the typical AOD at these places. In order to compare with satellite AOD variability, we performed a case study using MODIS/AQUA 1 km AOD from MAIAC algorithm over Beijing and REUNION_ST_DENIS (see Appendix).

The AE is a qualitative indicator of aerosol particle size; the smaller the AE, the larger the particle size [50,51]. The spatial variability of AE is high over sites where both the fine and coarse mode particles have strong effects. The mean SV_{AE}(440/870 nm) is 0.012 per km (1σ=0.012). The distribution of the SV_{AE} over 30 AERONET sites is shown in Fig. 6b. The highest value is observed over #19 Thessaloniki with ~0.049/km, where coarse mode oceanic aerosol and fine mode urban aerosol alternate dominance. Multiplicating by a factor of four the SV_{AE}, then the AE variability over 4 km is on average ~0.048 over 30 sites with the highest value ~0.2. For SV_{AE}, we found high AE temporal variability over Lanai #30 ~0.051 per hour, but here the spatial variability is low (~0.003 per km), which means that the aerosol particle size varies quickly in time due to high wind speed; however, high wind speed also spatially distributes aerosol homogeneously.

The mean SV_{SSA}(440 nm) is 0.001 per km (1σ=0.001). Fig. 6c shows the SSA spatial variability over 30 AERONET sites. The highest SV_{SSA}(440 nm) is observed at #19 Thessaloniki with ~0.006/km, and the lowest values are at #30 Lanai with

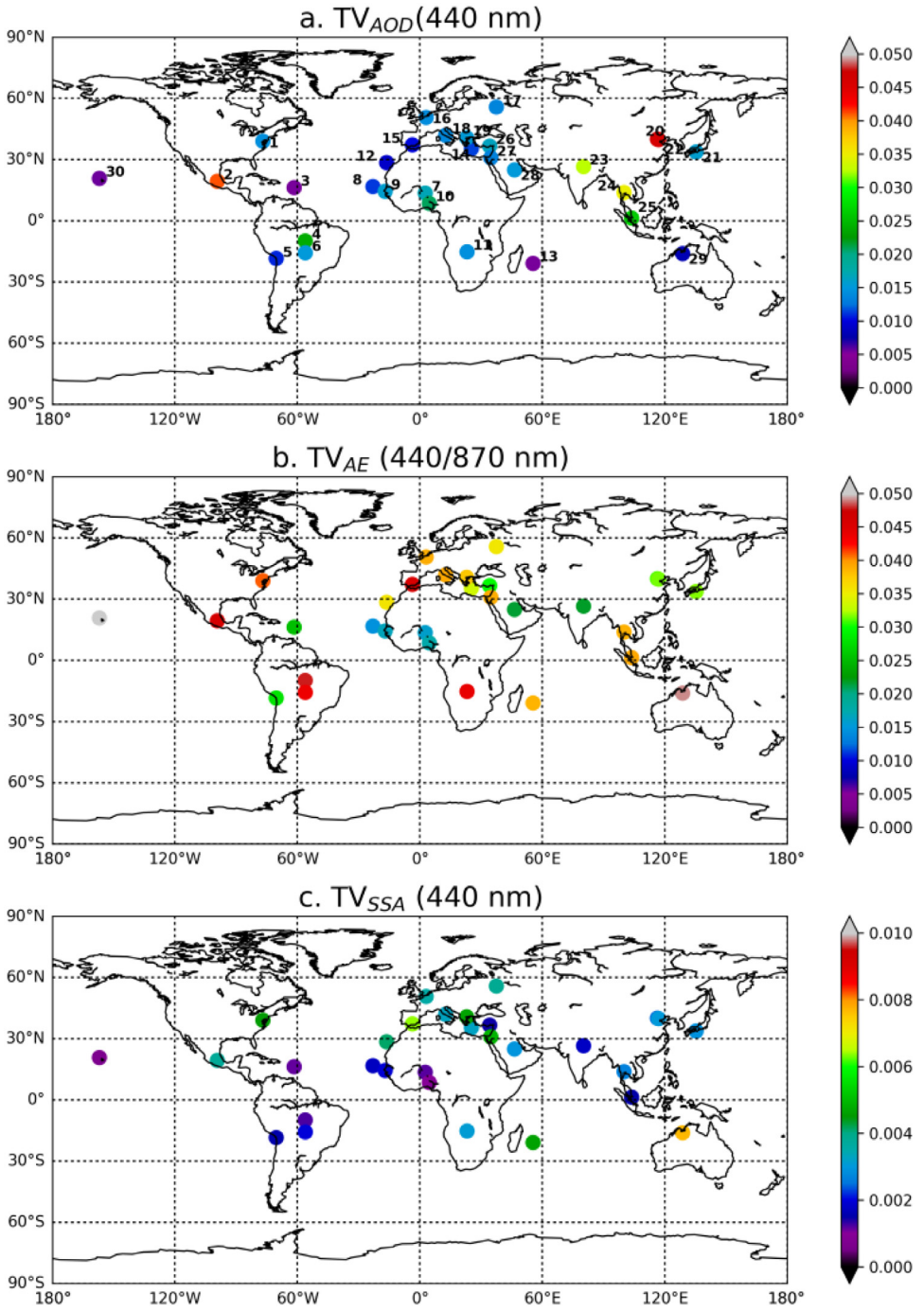

Fig. 5. Aerosol temporal variability represented in Panel a. by TV_{AOD}(440 nm), in Panel b. by TV_{AE}(440/870 nm) and in Panel c. by TV_{SSA}(440 nm), over 30 AERONET sites. The site numbers correspond to the #ID in Table 1.

~0.00005/km and #3 Guadeloup with ~0.00006/km. Even when converting the SSA (440 nm) spatial variability to 4 km scales, by multiplying a factor of 4 the ΔSSA_{SV}(440 nm), the mean variability is 0.008 and the highest value observed is ~0.032, which is within or comparable to the retrieval uncertainty of the SSA (±0.03). Overall, the SSA variability is small at scales varying from 1 to 4 km.

4.3. Aerosol mean variability difference from 2 km to 4 km

Here we discuss the results of the aerosol variability between mean AODs calculated for 2 km and 4 km grid boxes. Specifically, the $MSVD_{AOD}$, $MSVD_{AE}$ and $MSVD_{SSA}$ were estimated for the square grid box of 2 km and larger grid boxes extending up to 4 km. The $MSVD_{AOD}$, $MSVD_{AE}$ and $MSVD_{SSA}$ are the most appropriate parameters, for characterizing mean aerosol values, for evaluating the potential uncertainty introduced by changing the sampling resolution from 2 to 4 km scale. The $MSVD_{AOD}$, $MSVD_{AE}$ and $MSVD_{SSA}$ were calculated for 30 selected AERONET and the details are provided below.

The $MSVD_{AOD}$(440 nm) over 30 AERONET sites is shown in Fig. 7a. The average $MSVD_{AOD}$(440 nm) over all sites is 0.004 (1σ=0.005). The highest $MSVD_{AOD}$(440 nm) is observed over #20 Beijing at ~0.019, which represents ~2.8% of the mean AOD (440

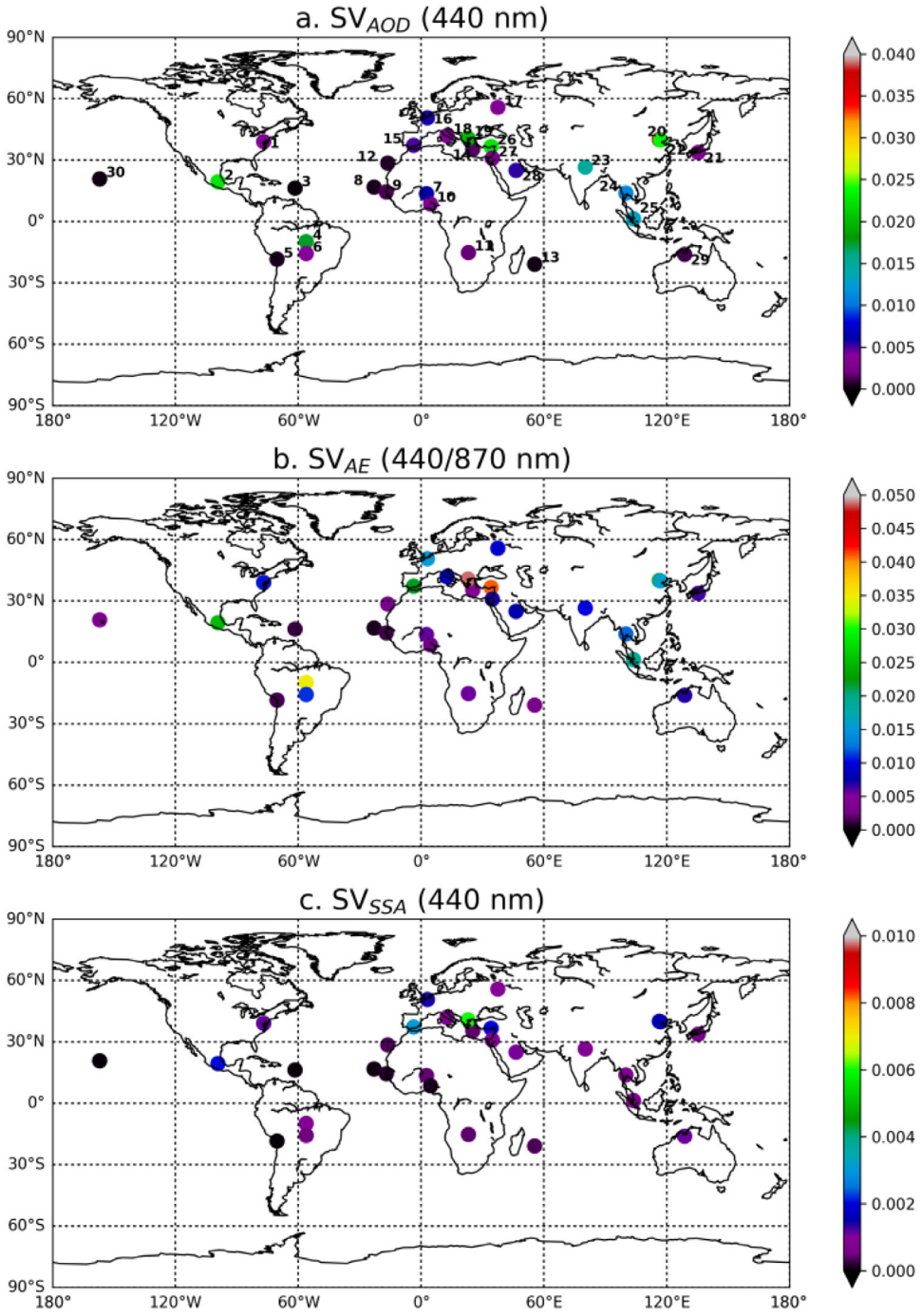

Fig. 6. Aerosol spatial variability, a. SV_{AOD}(440 nm), b. SV_{AE}(440/870 nm) and c. SV_{SSA}(440 nm) (top to bottim), over 30 AERONET sites. The site numbers correspond to the #ID in Table 1.

nm) over Beijing. Over other urban sites, such as #1 GSFC, #2 Mexico_City, #22 Xianghe and #23 Kanpur, the $MSVD_{AOD}$(440 nm) is slightly higher than 0.01. Nevertheless, even the highest value of ~0.019 over Beijing is within the practical uncertainty of AOD measurements by AERONET (±0.01-0.02). In conclusion, the uncertainties of this level in AOD variability can be considered nearly negligible.

The average $MSVD_{AE}$(440/870 nm) over 30 sites is 0.004 (1σ=0.003), which is ~0.4% of the mean AE. The $MSVD_{AE}$ over all AERONET sites is shown in Fig. 7b. The highest AE variability is over sites affected by biomass buring, e.g. at #11 Mongu the $MSVD_{AE}$ is ~0.011 (0.6% of the mean) and at #24 Silpakorn Univ it is ~0.014 (1.0% of the mean), which can be understood by the fact that air affected by biomass burning is dominated by fine particles leading to high AE values. At the same time, even these apparently high values are within the AE uncertainty limits (± 0.1–0.3) of AERONET.

The average $MSVD_{SSA}$(440 nm) over 30 sites is 0.001 (1σ=0.001), which is smaller than 0.1% of the mean SSA. The $MSVD_{SSA}$ over all AERONET sites is shown in Fig. 7c. Similar to $MSVD_{AOD}$(440 nm), the highest values of $MSVD_{SSA}$(440 nm) are mainly observed over urban and biomass burning affected sites, such as at #20 Beijing with ~0.002, at #6 CUIABA-MIRANDA with ~0.001 and at #4 Alta_Floresta with ~0.001. Nevertheless,

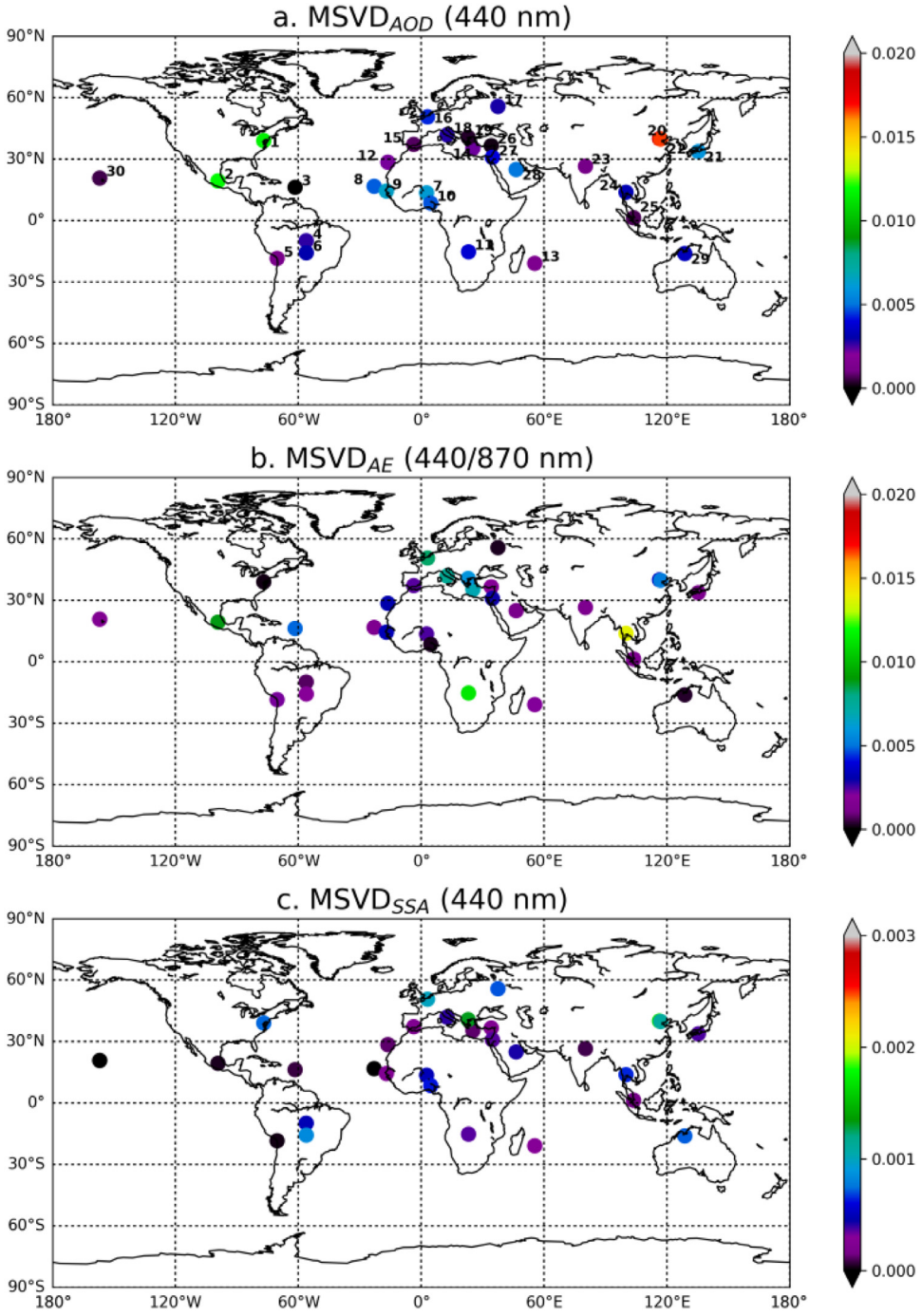

Fig. 7. Aerosol spatial variability, a. $MSVD_{AOD}$(440 nm), b. $MSVD_{AE}$(440/870 nm) and c. $MSVD_{SSA}$(440 nm) (top to bottim), over 30 AERONET sites. The site numbers correspond to the #ID in Table 1.

similarly to situation with $MSVD_{AOD}$ and $MSVD_{AE}$, the values of $MSVD_{SSA}$ are clearly within the SSA uncertainty limits (±0.03) of AERONET.

The mean spatial variability between 2 km and 4 km grid boxes ($MSVD_{AOD}$, $MSVD_{AE}$ and $MSVD_{SSA}$) are generally lower than the aerosol variability at 4 km scale, multiplying by a factor 4 the SV_{AOD}, SV_{AE} and SV_{SSA}, which can be interpreated as aerosol variability per 4 km in Section 4.2. This is due to that aerosol spatial variability is calculated from maximum temporal variability during the time windows. Nevertheless, the mean spatial variability between 2 km and 4 km grid boxes are derived differences of the mean variability for 2 time windows representing for 2 km and 4 km (Eq. (7)).

Table 2 summarizes the statistics of aerosol (AOD(440 nm), AE(440/870) and SSA(440 nm)) temporal variability (Δ/h), spatial variability (Δ/km) and mean difference in spatial variability between 2 km and 4 km grid boxes $\overline{\Delta(4\text{km} - 2\text{km})}$ for all 30 AERONET sites. Fig. 8 shows a qualitative insight obtained by using a straightforward clustering analysis of aerosol temporal (Fig. 8a-c), spatial (Fig. 8e-g) and mean difference in spatial variability from 2 to 4 km (Fig. 8i-k). One can observe that the highest TV_{AOD} values are observed for urban polluted and biomass burning affected

Table 2
Statistics of aerosol (AOD(440 nm), AE(440/870) and SSA(440 nm)) temporal variability (Δ/h), spatial variability (Δ/km) and mean spatial variability between 2 km and 4 km grid boxes $\overline{\Delta(4\text{km} - 2\text{km})}$ over 30 AERONET sites.

	Temporal variability (Δ/h)			Spatial variability (Δ/km)			$\overline{\Delta(4\text{km} - 2\text{km})}$		
	TV_{AOD}	TV_{AE}	TV_{SSA}	SV_{AOD}	SV_{AE}	SV_{SSA}	$MSVD_{AOD}$	$MSVD_{AE}$	$MSVD_{SSA}$
Mean	0.018	0.034	0.003	0.008	0.012	0.001	0.004	0.004	0.0005
Upper (20%)	0.038	0.047	0.005	0.024	0.033	0.002	0.012	0.009	0.001
Lower (20%)	0.007	0.018	0.001	0.001	0.002	0.0001	0.0004	0.0005	<0.0001
Maximum	0.049	0.051	0.008	0.036	0.049	0.006	0.019	0.014	0.002

Note. AOD and SSA are reported at 440 nm, and AE is 440/870 nm.

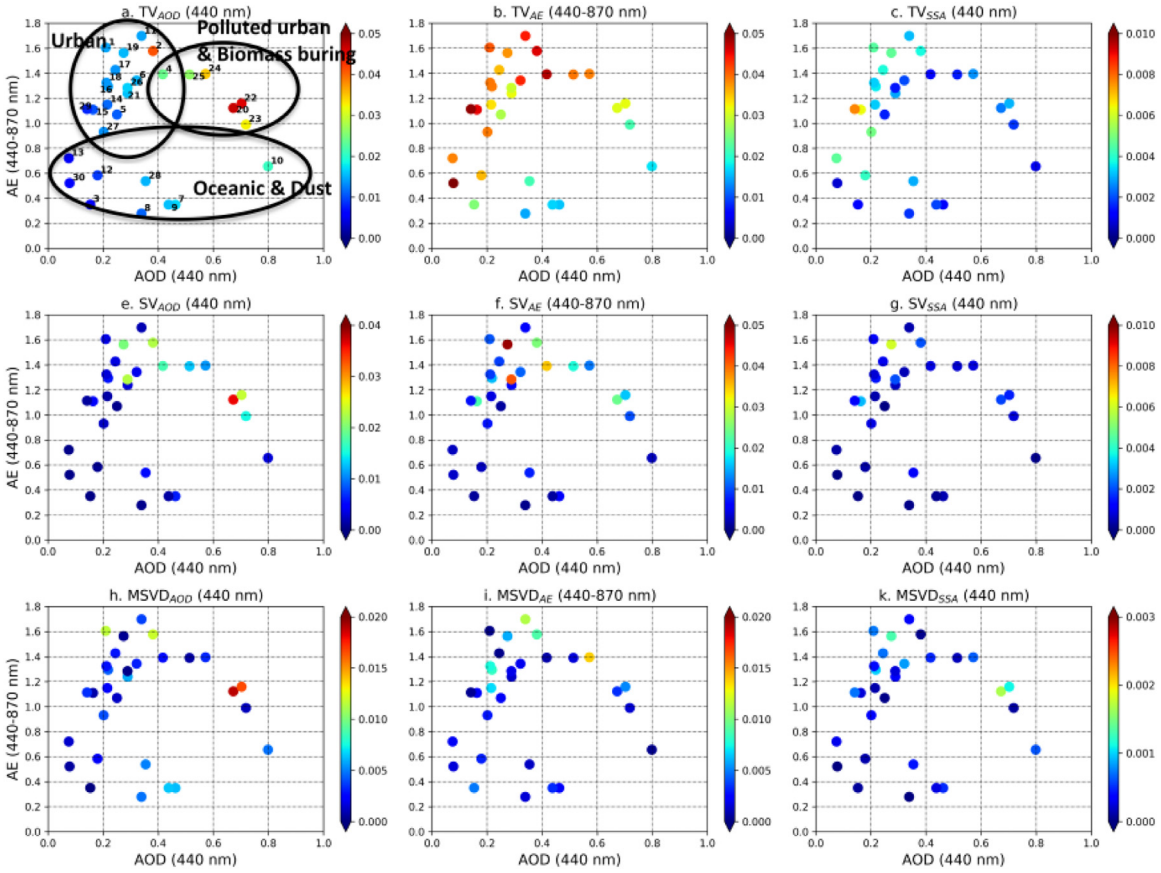

Fig. 8. Clustering analysis of aerosol temporal, spatial and mean spatial variability difference from 2 to 4 km over 30 AERONET sites; the site numbers are present in (panel a). The x-axis and y-axis are mean AOD (440 nm) vs. mean AE (440/870 nm) for 30 sites, and the color represents aerosol temporal (a-c), spatial (e-g) and mean spatial variability (i-k).

sites, which are generally characterized by high aerosol loading and variability [2]. The highest TV_{AE} values are observed for urban polluted sites, which are known to observe mixtures of fine and coarse mode aerosols with high AE dynamics. The TV_{AE} values are also high for sites with low AOD, which are evidently related to the uncertainty of the underlying AOD observations (±0.01-0.02). Correspondingly, at very low AOD, the AE can strongly vary simply due to these uncertainties. The highest TV_{SSA} values are observed for urban polluted and biomass burning affected sites, which generally exhibit stronger SSA changes due to enhanced absorption by these aerosols [2]. In addition, it is interesting to note that the highest values of TV_{AOD}, TV_{AE} and TV_{SSA} correspond to the cases with the lowest wind speed (see Fig. 3). Evidently, in absence of strong winds the activity of local aerosol sources results in high temporal aerosol variability.

By considering the upper 20% of maximum mean spatial variability at 4 km (Δ/km x 4), the variability is less than 0.1 for AOD, 0.15 for AE and 0.02 for SSA. In addition, for mean difference in variability between 2 km to 4 km ($\overline{\Delta(4\text{km} - 2\text{km})}$), the mean of upper 20% cases are 0.012 for AOD, 0.009 for AE and 0.001 for SSA. Overall, for these case with extreme high aerosol loading, by accounting for the maximum variability at 4 km, the AOD variability could become non-negligible; however, the mean AOD variability for these extreme cases are within the uncertainty range (±0.01-0.02). For aerosol size and absorption parameters (AE and SSA), the variability is insignificant.

4.4. Aerosol temporal variability for polar-oribiting satellites overpass at 10 – 14 hrs localtime

The above analysis was derived by using all available AERONET data observed during daytime. The derived variability we can interpreat as daily mean. Smirnov et al. [52] discussed AOD diurnal variability for various aerosol types (e.g. urban pollution, dust, biomass buring, maritime etc.). A prevailing pattern was found that the AOD increases by 10-40% during the day, therefore the AOD

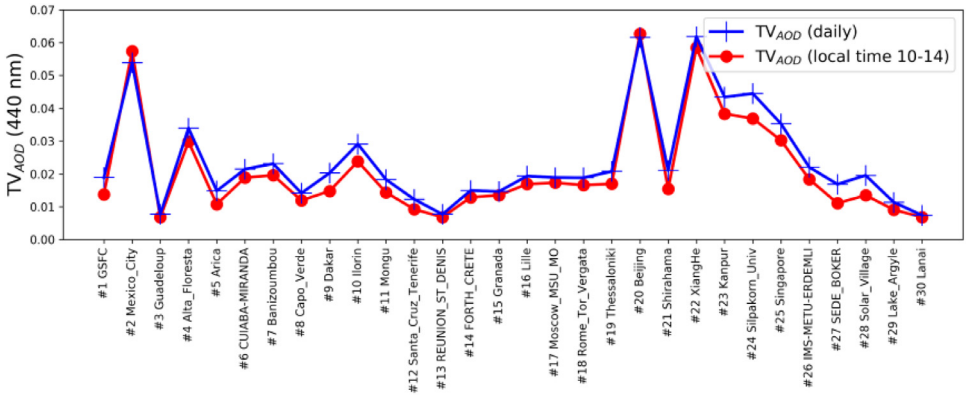

Fig. 9. Comparison of daily mean TV_{AOD}(440 nm) with TV_{AOD}(440 nm) at noon (localtime 10-14).

peak is mainly occurring in the afternoon, for most sites the exception for sites dominated by dust, where this trend is insignificant. Kanfman et al. [53] compared the daily mean AOD with the AOD of collocated observations from polar oribiting satellites, and found that the differences are insiginificant.

In order to understand the representiveness of derived daytime aerosol variability for the purpose of typical polar-oribit satellites overpass times (i.e. localtime between 10:00 and 14:00 hrs), we compare the daytime aerosol temporal variability TV_{AOD}(440 nm) derived using all data with the TV_{AOD} derived using data collected during the specific local time window between 10:00 and 14:00 hrs. The results are illustrated in Fig. 9: blue crosses are daily mean TV_{AOD}(440 nm) derived using all data; red circles are TV_{AOD}(440 nm) derived using data during the specific time window. In general, the TV_{AOD}(440 nm) during local time 10-14 is slightly lower than the dirual mean by 12.5% (local time 10-14: 0.021/h; dirual: 0.024/h). Two urban polluted sites (#2 Mexico_City and #20 Beijing) show that the variability around noon (local time 10-14) is higher than the daily mean variability by 6.6% (#2) and 1.8% (#20) respectively. In contrast, over dust sites (e.g. #9 Dakar, #27 SEDE_BOKER, #28 Solar_Village), the variability around noon is lower than the daily mean variability about 30%. These phonomena can be related to local emission variability and meteorological conditions, which would require further investigation. Neverthless, the difference between the temporal variability around noon and the daily mean temporal variability appears not evident.

5. Conclusions

In this study, we made an attempy to estimate the aerosol maximum temporal variability using full data archives of 30 representative AERONET sites. By exploiting additional information about local wind speed, the maximum and mean aerosol variability was estimated at scales of 2 km and 4 km, and then inverstigated for clear differences that could affect satellite requirements. The results of this study can be summarized by the following conclusions:

- √ Aerosol maximum temporal variability (Δ/h) is influenced by local wind speed. For example, the AOD temporal variability is high over urban polluted sites where the local wind speed is low. On the other hand, the aerosol size parameter (AE) shows high temporal variability over oceanic sites where the local wind speed is high. The aerosol temporal variability in 1 hour is generally higher than its spatial variability at 1 km.
- √ The changes of aerosol type, which is linked in this study to changes in AE and SSA, can be considered negligible or tolerable at spatial scales of 4 km. For example, over 30 sites the maximum variability of the TV_{AE}(440/870 nm) at 4 km is 0.196; and the maximum variability of the TV_{SSA}(440 nm) at 4 km is 0.032. These values are comparable with the measurements accuracy limits of AE and SSA ($\pm$0.1-0.3 for AE and $\pm$0.03 for SSA) in AERONET.
- √ The mean (over 30 sites) maximum AOD (440 nm) spatial variability within a scale of 4 km is 0.032, with highest maximum variability of AOD observed over urban polluted sites such as #20 Beijing, #22 Xianghe, #2 Mexico_City and #23 Kanpur where the maximum values reach ~0.1-0.2, which is quite significant. The corresponding values for maximum aerosol variability for the scale of 2 km are two times smaller. At the same time, the highest AOD variability observed at the sites with very high dynamic of aerosol and AOD variability per km is associated with only ~6% relative changes in AOD.
- √ In order to understand more adequately the impact of changes at satellite sampling resolution changing from 2 km to 4 km, we have analyzed the differences in the mean values of aerosol properties (AOD, AE and SSA) estimated for 2 km and 4 km grid box sizes. It is to be expected that mainly the average aerosol properties within these grid boxes would affect the satellite observations. The results can be summarized as follows:
  - Mean difference of AOD (440 nm) variability between 2 km and 4 km grid boxes is only 0.004 (1σ=0.005), which is corresponding to 1.2% of the mean AOD value in the grid box. The highest differences between 2 km and 4 km mean AOD (440 nm) are mainly found over urban sites such as #20 Beijing 0.019 (2.8%), where typical values of AOD are very high.
  - Mean difference of AE (440/870 nm) variability between 2 km and 4 km grid boxes is 0.004 (1σ=0.003), which is equivalent to 0.4% relative AE (440/870 nm). The highest AE (440/870 nm) variability from 2 km to 4 km is observed over biomass burning sites, e.g. #11 Mongu ~0.011 (0.6%) and #24 Silpakorn_Univ ~0.014 (1.0%).
  - Mean difference of SSA (440 nm) variability between 2 km and 4 km grid boxes is 0.001 (1σ=0.001), which is smaller than 0.1% of the mean SSA, and the highest SSA variability is found over urban sites.

All the observed mean aerosol variability differences between 2 km and 4 km grid box sizes for AOD, AE and SSA are comparable with the limits of AERONET AOD, AE and SSA measurement accuracies ($\pm$0.01-0.03 for AOD, $\pm$0.1-0.3 for AE, $\pm$0.03 for SSA). The analysis as presented here leads to recommend that using 4 km spatial resolution for the MAP sensor on the CO2M Mission will be sufficient to capture the most important characteristics in aerosol variability. This conclusion is important especially taking into account the fact that due to fundamental limitations of multi-angular measurements from space providing high quality consistent MAP

observations at 4 km scale is significantly less challenging than for higher spatial resolution sensors that is because other errors in relation to geometrical co-registration of MAP observations will become significantly more prominent at higher spatial resolution.

Declaration of Competing Interest

The authors declare that they have no known competing financial interests or personal relationships that could have appeared to influence the work reported in this paper.

CRediT authorship contribution statement

Cheng Chen: Methodology, Formal analysis, Investigation, Writing – original draft. **Oleg Dubovik:** Conceptualization, Methodology, Writing – review & editing. **Gregory L. Schuster:** Methodology, Writing – review & editing. **David Fuertes:** Methodology, Software, Investigation, Writing – review & editing. **Yasjka Meijer:** Writing – review & editing, Funding acquisition. **Jochen Landgraf:** Funding acquisition. **Yana Karol:** Writing – review & editing, Project administration. **Zhengqiang Li:** Methodology, Writing – review & editing.

Acknowledgement

This study was supported by the European Space Agency, ESTEC under the contract of the Study on Spectral Sizing for CO_2 Observation No. 4000118601/16/NL/FF/gp. We would like to acknowledge the AERONET team and MERRA-2 team for making their data available for the community. All PIs of AERONET sites are gratefully acknowledged.

Appendix

In order to evaluate the potential of using MAIAC 1 km resolution product for evaluation of aerosol spatial variability we performed a case study using MODIS/AQUA MAIAC AOD over Beijing and REUNION_ST_DENIS, where we got the maximum and minimal AOD spatial variability (SV_{AOD}) using AERONET and MERRA-2 wind speed in Section 4.2. The results and compassion with the SV_{AOD} derived in this study are presented in Fig. A1 and Table A1.

We adopted a year data in 2008, and only the MAIAC AOD with the highest quality flag (QA="0000") was used. The spatial distribution of MAIAC 1 km AOD (550 nm) is shown in Fig. A1. We calculated the maximum absolute AOD changes for the AERONET pixel with its surrounding pixels within 1 km distance. As a result, we have obtained a value of SV_{AOD_MAIAC} (550nm) 0.037, and the relative change with respect to mean AOD (550nm) is 9.8%. It should be noted also that the AOD variability for MAIAC is derived only at 550 nm. Even though, we used the data over Beijing for different time period (AERONET: 2001-2019; MAIAC: 2008), the AOD variability per km is comparable (AERONET: 0.036 at 440 nm; MAIAC: 0.037 at 550 nm). The relative changes for MAIAC

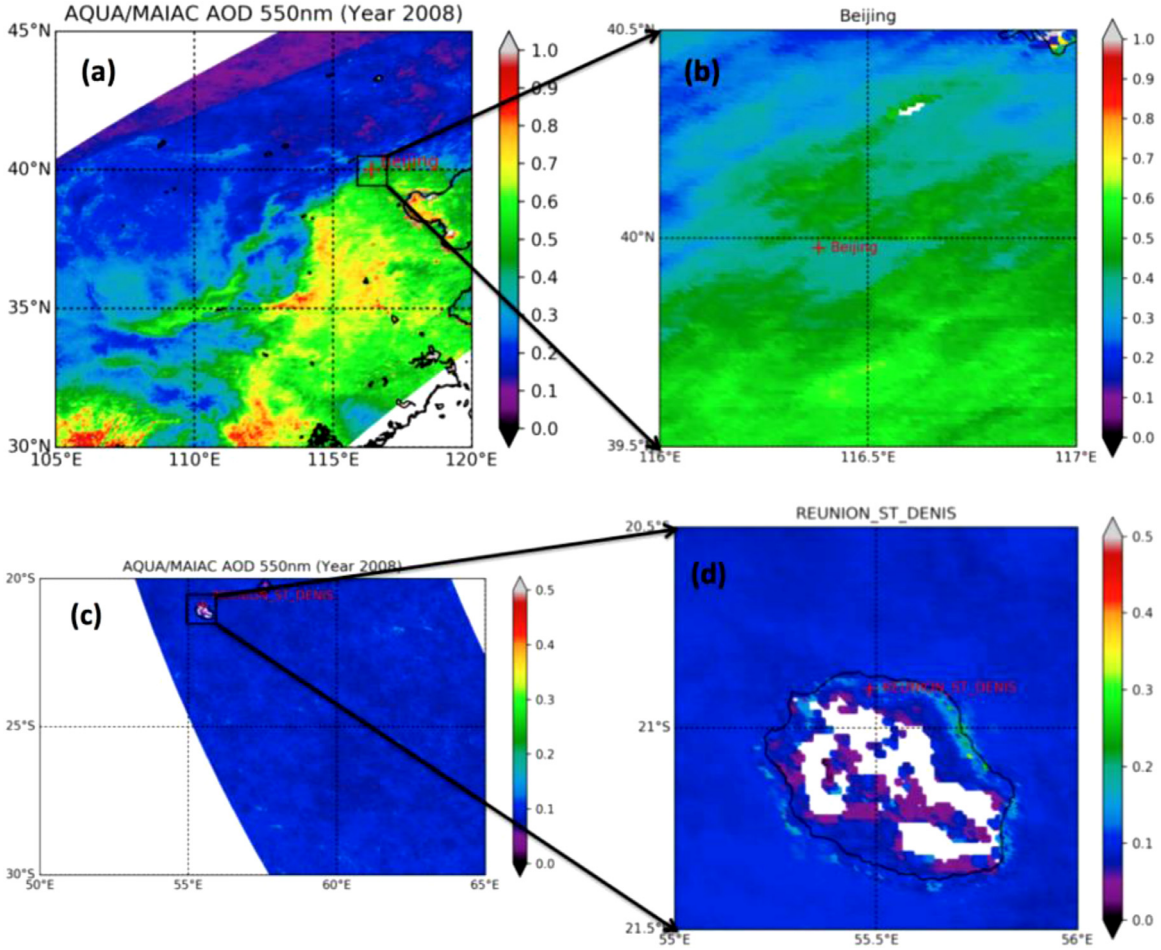

Fig. A1. (a) Spatial distribution of annual mean AQUA/MAIAC 1 km AOD (550 nm) over North China in 2008. (b) Zoom in MAIAC 1 km AOD (550 nm) on a 1 degree grid cell centered on AERONET site "Beijing". (c) Spatial distribution of annual mean AQUA/MAIAC 1 km AOD (550 nm) over REUNION_ST_DENIS. (d) Zoom in MAIAC 1 km AOD (550 nm) on a 1 degree grid cell centered on AERONET site "REUNION_ST_DENIS". The red crosses indicate the AERONET site Beijing (116.381°E, 39.977°N) in (a) and (b) and AERONET site REUNION_ST_DENIS (55.485°E, 20.901°S) in (c) and (d).

Table A1
Comparison the AOD spatial variability (SV_{AOD}) per km and AOD relative changes to the mean over Beijing and REUNION_ST_DENIS derived from MAIAC AOD with AERONET + MERRA-2 wind speed in Section 4.2.

	AOD Spatial Variability per km (relative changes to mean: %)	
	MAIAC SV_{AOD}	AERONET + MERRA-2 wind speed SV_{AOD}
Beijing	0.037 (9.8%)	0.036 (5.5%)
REUNION_ST_DENIS	0.004 (5.5%)	0.0004 (0.5%)

(9.8%) that is slightly higher than the one (5.5%) derived from AERONET data (using MERRA-2 wind speed), which could partially be explained also by the fact that the MAIAC AOD is slightly lower than AERONET measurements over Beijing. Meanwhile, we got SV_{AOD_MAIAC} (550nm) 0.004, and the relative change is 5.5% at REUNION_ST_DENIS (Fig. A1), where the aerosol loading is generally low (AERONET mean AOD at 440 nm is 0.08). The derived SV_{AOD} using AERONET and MERRA-2 wind speed is 0.0004 per km (0.5% in relative change), which is 10 times smaller than the SV_{AOD_MAIAC} (550nm). The higher MAIAC AOD variability can probably be explained that MODIS AOD can be affected by other factors such as surface heterogeneity and topology especially in cases with low aerosol loading. At the same time, these obtained values of variability are much smaller even than the AERONET AOD uncertainty (±0.01-0.02), which is known to be the AOD products of the highest quality and certainly much smaller than expected MAIAC AOD accuracy. The interpretation of such differences in the results obtained from AERONET based and MAIAC MODIS based data is challenging and rather ambiguous.

References

[1] Eck TF, Holben BN, Reid JS, Sinyuk A, Dubovik O, Smirnov A, Giles D, O'Neill NT, Tsay S-C, Ji Q, Al Mandoos A, Ramzan Khan M, Reid EA, Schafer JS, Sorokine M, Newcomb W, Slutsker I. Spatial and temporal variability of column-integrated aerosol optical properties in the southern Arabian Gulf and United Arab Emirates in summer. J Geophys Res 2008;113(D1):D01204. doi:10.1029/2007JD008944.

[2] Dubovik O, Holben B, Eck TF, Smirnov A, Kaufman YJ, King MD, Tanré D, Slutsker I. Variability of absorption and optical properties of key aerosol types observed in worldwide locations. J Atmos Sci 2002;59(3):590–608. doi:10.1175/1520-0469(2002)059⟨0590:VOAAOP⟩2.0.CO;2.

[3] Pöschl U. Atmospheric aerosols: Composition, transformation, climate and health effects. Angew Chemie - Int Ed 2005;44:7520–40. doi:10.1002/anie.200501122.

[4] Rosenfeld D, Sherwood S, Wood R, Donner L. Climate effects of aerosol-cloud interactions. Science 2014;343(80-):379–80. doi:10.1126/science.1247490.

[5] Sarnat SE, Klein M, Sarnat JA, Flanders WD, Waller LA, Mulholland JA, et al. An examination of exposure measurement error from air pollutant spatial variability in time-series studies. J Expo Sci Environ Epidemiol 2010;20:135–46. doi:10.1038/jes.2009.10.

[6] Shiraiwa M, Ueda K, Pozzer A, Lammel G, Kampf CJ, Fushimi A, et al. Aerosol health effects from molecular to global scales. Environ Sci Technol 2017;51:13545–67. doi:10.1021/acs.est.7b04417.

[7] Yu H, Chin M, Bian H, Yuan T, Prospero JM, Omar AH, Remer LA, Winker DM, Yang Y, Zhang Y, Zhang Z. Quantification of trans-Atlantic dust transport from seven-year (2007-2013) record of CALIPSO lidar measurements. Remote Sens Environ. 2015;159:232–49. doi:10.1016/j.rse.2014.12.010.

[8] Chen C, Dubovik O, Fuertes D, Litvinov P, Lapyonok T, Lopatin A, Ducos F, Derimian Y, Herman M, Tanré D, Remer LA, Lyapustin A, Sayer AM, Levy RC, Hsu NC, Descloitres J, Li L, Torres B, Karol Y, Herrera M, Herreras M, Aspetsberger M, Wanzenboeck M, Bindreiter L, Marth D, Hangler A, Federspiel C. Validation of GRASP algorithm product from POLDER/PARASOL data and assessment of multi-angular polarimetry potential for aerosol monitoring. Earth Syst Sci Data 2020;12:3573–620. doi:10.5194/essd-12-3573-2020.

[9] Dubovik O, Li Z, Mishchenko MI, Tanré D, Karol Y, Bojkov B, Cairns B, Diner DJ, Espinosa WR, Goloub P, Gu X, Hasekamp O, Hong J, Hou W, Knobelspiesse KD, Landgraf J, Li L, Litvinov P, Liu Y, Lopatin A, Marbach T, Maring H, Martins V, Meijer Y, Milinevsky G, Mukai S, Parol F, Qiao Y, Remer L, Rietjens J, Sano I, Stammes P, Stamnes S, Sun X, Tabary P, Travis LD, Waquet F, Xu F, Yan C, Yin D. Polarimetric remote sensing of atmospheric aerosols: instruments, methodologies, results, and perspectives. J Quant Spectrosc Radiat Transf 2019;224:474–511. doi:10.1016/J.JQSRT.2018.11.024.

[10] Fougnie B, Marbach T, Lacan A, Lang R, Schlüssel P, Poli G, Munro R, Couto AB. The multi-viewing multi-channel multi-polarisation imager – Overview of the 3MI polarimetric mission for aerosol and cloud characterization. J Quant Spectrosc Radiat Transf 2018;219:23–32. doi:10.1016/j.jqsrt.2018.07.008.

[11] Janssens-Maenhout G, Pinty B, Dowell M, Zunker H, Andersson E, Balsamo G, Bézy J-L, Brunhes T, Bösch H, Bojkov B, Brunner D, Buchwitz M, Crisp D, Ciais P, Counet P, Dee D, Denier van der Gon H, Dolman H, Drinkwater M, Dubovik O, Engelen R, Fehr T, Fernan-dez V, Heimann M, Holmlund K, Houweling S, Husband R, Juvyns O, Kentarchos A, Land-graf J, Lang R, Löscher A, Marshall J, Meijer Y, Nakajima M, Palmer PI, Peylin P, Rayner P, Scholze M, Sierk B, Tamminen, qnd J, Veefkind P. Towards an operational anthropogenic CO2 emissions monitoring and verification support capacity. Bull Am Meteorol Soc 2020. doi:10.1175/BAMS-D-19-0017.1.

[12] Li Z, Hou W, Hong J, Zheng F, Luo D, Wang J, Gu X, Qiao Y. Directional polarimetric camera (DPC): monitoring aerosol spectral optical properties over land from satellite observation. J Quant Spectrosc Radiat Transf 2018;218:21–37. doi:10.1016/J.JQSRT.2018.07.003.

[13] Rusli SP, Hasekamp O, Aan de Brugh J, Fu G, Meijer Y, Landgraf J. Anthropogenic CO2 monitoring satellite mission: the need for multi-angle polarimetric observations. Atmos Meas Tech Discuss 2020. 1–31, [online] Available from: https://www.atmos-meas-tech-discuss.net/amt-2020-152/ .

[14] Lang R, Poli G, Fougnie B, Lacan A, Marbach T, Riedi J, Schlüssel P, Couto AB, Munro R. The 3MI Level-1C geoprojected product – definition and processing description. J. Quant. Spectrosc. Radiat. Transf. 2019;225:91–109 2019. doi:10.1016/j.jqsrt.2018.12.022.

[15] Chin M, Diehl T, Ginoux P, Malm W. Intercontinental transport of pollution and dust aerosols: implications for regional air quality. Atmos Chem Phys 2007;7(21):5501–17. doi:10.5194/acp-7-5501-2007.

[16] Kaufman YJ, Koren I, Remer LA, Tanré D, Ginoux P, Fan S. Dust transport and deposition observed from the Terra-Moderate resolution imaging spectroradiometer (MODIS) spacecraft over the Atlantic ocean. J Geophys Res D Atmos. 2005;110(10):1–16. doi:10.1029/2003JD004436.

[17] Kim D, Chin M, Yu H, Pan X, Bian H, Tan Q, Kahn RA, Tsigaridis K, Bauer SE, Takemura T, Pozzoli L, Bellouin N, Schulz M. Asian and Trans-Pacific dust: a multimodel and multiremote sensing observation analysis. J Geophys Res Atmos. 2019;124(23):13534–59. doi:10.1029/2019JD030822.

[18] Chin M, Diehl T, Tan Q, Prospero JM, Kahn RA, Remer LA, Yu H, Sayer AM, Bian H, Geogdzhayev IV, Holben BN, Howell SG, Huebert BJ, Hsu NC, Kim D, Kucsera TL, Levy RC, Mishchenko MI, Pan X, Quinn PK, Schuster GL, Streets DG, Strode SA, Torres O, Zhao X-P. Multi-decadal aerosol variations from 1980 to 2009: a perspective from observations and a global model. Atmos Chem Phys 2014;14(7):3657–90. doi:10.5194/acp-14-3657-2014.

[19] Mahowald N, Luo C, del Corral J, Zender CS. Interannual variability in atmospheric mineral aerosols from a 22-year model simulation and observational data. J Geophys Res Atmos 2003;108(12). doi:10.1029/2002jd002821.

[20] De Meij A, Pozzer A, Lelieveld J. Trend analysis in aerosol optical depths and pollutant emission estimates between 2000 and 2009. Atmos Environ 2012;51:75–85. doi:10.1016/j.atmosenv.2012.01.059.

[21] Mishchenko MI, Geogdzhayev IV, Rossow WB, Cairns B, Carlson BE, Lacis AA, Liu L, Travis LD. Long-term satellite record reveals likely recent aerosol trend. Science 2007;315(5818):1543. doi:10.1126/science.1136709.

[22] Pozzer A, de Meij A, Yoon J, Tost H, Georgoulias AK, Astitha M. AOD trends during 2001–2010 from observations and model simulations. Atmos Chem Phys 2015;15(10):5521–35. doi:10.5194/acp-15-5521-2015.

[23] Zhao B, Jiang JH, Diner DJ, Su H, Gu Y, Liou K-N, Jiang Z, Huang L, Takano Y, Fan X, Omar AH. Intra-annual variations of regional aerosol optical depth, vertical distribution, and particle types from multiple satellite and ground-based observational datasets. Atmos Chem Phys 2018;18:11247–60. doi:10.5194/acp-18-11247-2018.

[24] Eck TF, Holben BN, Reid JS, Sinyuk A, Hyer EJ, O'Neill NT, Shaw GE, Vande Castle JR, Chapin FS, Dubovik O, Smirnov A, Vermote E, Schafer JS, Giles D, Slutsker I, Sorokine M, Newcomb WW. Optical properties of boreal region biomass burning aerosols in central Alaska and seasonal variation of aerosol optical depth at an Arctic coastal site. J Geophys Res Atmos 2009;114(11):1–14. doi:10.1029/2008JD010870.

[25] Remer LA, Kleidman RG, Levy RC, Kaufman YJ, Tanré D, Mattoo S, Martins JV, Ichoku C, Koren I, Yu H, Holben BN. Global aerosol climatology from the MODIS satellite sensors. J Geophys Res 2008;113(D14):D14S07. doi:10.1029/2007JD009661.

[26] Anderson TL, Charlson RJ, Winker DM, Ogren JA, Holmén K. Mesoscale variations of tropospheric aerosols. J Atmos Sci 2003;60:119–36. doi:10.1175/1520-0469(2003)060⟨0119:MVOTA⟩2.0.CO;2.

[27] Chudnovsky AA, Kostinski A, Lyapustin A, Koutrakis P. Spatial scales of pollution from variable resolution satellite imaging. Environ Pollut 2013;172:131–8. doi:10.1016/j.envpol.2012.08.016.

[28] Chudnovsky A, Tang C, Lyapustin A, Wang Y, Schwartz J, Koutrakis P. A critical assessment of high-resolution aerosol optical depth retrievals for fine par-

ticulate matter predictions. Atmos Chem Phys 2013;13:10907–17. doi:10.5194/acp-13-10907-2013.
[29] Chudnovsky AA, Koutrakis P, Kloog I, Melly S, Nordio F, Lyapustin A, et al. Fine particulate matter predictions using high resolution aerosol optical depth (AOD) retrievals. Atmos Environ 2014;89:189–98. doi:10.1016/j.atmosenv.2014.02.019.
[30] Mei L, Strandgren J, Rozanov V, Vountas M, Burrows JP, Wang Y. A study of the impact of spatial resolution on the estimation of particle matter concentration from the aerosol optical depth retrieved from satellite observations. Int J Remote Sens 2019;40:7084–112. doi:10.1080/01431161.2019.1601279.
[31] Ichoku C, Allen Chu D, Mattoo S, Kaufman YJ, Remer LA, Tanré D, et al. A spatio-temporal approach for global validation and analysis of MODIS aerosol products. Geophys Res Lett 2002;29 MOD1-1-MOD1-4. doi:10.1029/2001GL013206.
[32] Redemann J, Zhang Q, Schmid B, Russell PB, Livingston JM, Jonsson H, et al. Assessment of MODIS-derived visible and near-IR aerosol optical properties and their spatial variability in the presence of mineral dust. Geophys Res Lett 2006;33:2–7. doi:10.1029/2006GL026626.
[33] Hsu NC, Jeong M-J, Bettenhausen C, Sayer AM, Hansell R, Seftor CS, Huang J, Tsay S-C. Enhanced deep blue aerosol retrieval algorithm: the second generation. J Geophys Res Atmos 2013;118(16):9296–315. doi:10.1002/jgrd.50712.
[34] Levy RC, Mattoo S, Munchak LA, Remer LA, Sayer AM, Patadia F, Hsu NC. The Collection 6 MODIS aerosol products over land and ocean. Atmos Meas Tech. 2013;6(11):2989–3034. doi:10.5194/amt-6-2989-2013.
[35] Remer LA, Mattoo S, Levy RC, Munchak LA. MODIS 3 km aerosol product: algorithm and global perspective. Atmos Meas Tech 2013;6:1829–44. doi:10.5194/amt-6-1829-2013.
[36] Lyapustin A, Wang Y, Korkin S, Huang D. MODIS collection 6 MAIAC algorithm. Atmos Meas Tech 2018;11:5741–65. doi:10.5194/amt-11-5741-2018.
[37] Hu X, Waller LA, Lyapustin A, Wang Y, Al-Hamdan MZ, Crosson WL, et al. Estimating ground-level PM2.5 concentrations in the Southeastern United States using MAIAC AOD retrievals and a two-stage model. Remote Sens Environ 2014;140:220–532. doi:10.1016/j.rse.2013.08.032.
[38] Kloog I, Chudnovsky AA, Just AC, Nordio F, Koutrakis P, Coull BA, et al. A new hybrid spatio-temporal model for estimating daily multi-year PM2.5 concentrations across northeastern USA using high resolution aerosol optical depth data. Atmos Environ 2014;95:581–90. doi:10.1016/j.atmosenv.2014.07.014.
[39] Holben BN, Eck TF, Slutsker I, Tanré D, Buis JP, Setzer A, Vermote E, Reagan JA, Kaufman YJ, Nakajima T, Lavenu F, Jankowiak I, Smirnov A. AERONET—a federated instrument network and data archive for aerosol characterization. Remote Sens Environ. 1998;66(1):1–16. doi:10.1016/S0034-4257(98)00031-5.
[40] Smirnov A, Holben BN, Eck TF, Dubovik O, Slutsker I. Effect of wind speed on columnar aerosol optical properties at Midway Island. J Geophys Res D Atmos 2003;108. doi:10.1029/2003jd003879.
[41] Kinne S, O'Donnel D, Stier P, Kloster S, Zhang K, Schmidt H, Rast S, Giorgetta M, Eck TF, Stevens B. MAC-v1: a new global aerosol climatology for climate studies. J Adv Model Earth Syst 2013;5(4):704–40. doi:10.1002/jame.20035.
[42] CO2M, MRD (Mission Requirements Document), Copernicus CO2 monitoring mission requirements document, version 3.0, European space agency (ESA), earth and mission science division, https://esamultimedia.esa.int/docs/EarthObservation/CO2M_MRD_v3.0_20201001_Issued.pdf, 2020.
[43] Gelaro R, McCarty W, Suárez MJ, Todling R, Molod A, Takacs L, Randles CA, Darmenov A, Bosilovich MG, Reichle R, Wargan K, Coy L, Cullather R, Draper C, Akella S, Buchard V, Conaty A, da Silva AM, Gu W, Kim G-K, Koster R, Lucchesi R, Merkova D, Nielsen JE, Partyka G, Pawson S, Putman W, Rienecker M, Schubert SD, Sienkiewicz M, Zhao B. The modern-era retrospective analysis for research and applications, version 2 (MERRA-2). J Clim 2017;30(14):5419–54. doi:10.1175/JCLI-D-16-0758.1.
[44] Dubovik O, King MD. A flexible inversion algorithm for retrieval of aerosol optical properties from Sun and sky radiance measurements. J Geophys Res Atmos 2000;105(D16):20673–96. doi:10.1029/2000JD900282.
[45] Dubovik O, Smirnov A, Holben BN, King MD, Kaufman YJ, Eck TF, Slutsker I. Accuracy assessments of aerosol optical properties retrieved from aerosol robotic network (AERONET) sun and sky radiance measurements. J Geophys Res Atmos 2000;105(D8):9791–806. doi:10.1029/2000JD900040.
[46] Dubovik O, Sinyuk A, Lapyonok T, Holben BN, Mishchenko M, Yang P, Eck TF, Volten H, Munoz O, Veihelmann B, van der Zander WJ, Sorokin M, Slutsker I. Application of spheroid models to account for aerosol particle nonsphericity in remote sensing of desert dust. J Geophys Res 2006;111:D11208. doi:10.1029/2005JD006619d.
[47] Giles DM, Sinyuk A, Sorokin MG, Schafer JS, Smirnov A, Slutsker I, Eck TF, Holben BN, Lewis JR, Campbell JR, Welton EJ, Korkin SV, Lyapustin AI. Advancements in the aerosol robotic network (AERONET) version 3 database – automated near-real-time quality control algorithm with improved cloud screening for Sun photometer aerosol optical depth (AOD) measurements. Atmos Meas Tech 2019;12(1):169–209. doi:10.5194/amt-12-169-2019.
[48] Carvalho D. An assessment of NASA's GMAO MERRA-2 reanalysis surface winds. J Clim 2019;32:8261–81. doi:10.1175/JCLI-D-19-0199.1.
[49] Holben, B. N., Eck, T. F., Slutsker, I., Smirnov, A., Sinyuk, A., Schafer, J., Giles, D. and Dubovik, O.: Aeronet's Version 2.0 quality assurance criteria, vol. 6408, edited by S.-C. Tsay, T. Nakajima, R. P. Singh, and R. Sridharan, p. 64080Q, international society for optics and photonics., 2006.
[50] Eck TF, Holben BN, Reid JS, Dubovik O, Smirnov A, O'Neill NT, Slutsker I, Kinne S. Wavelength dependence of the optical depth of biomass burning, urban, and desert dust aerosols. J Geophys Res Atmos. 1999;104(D24):31333–49. doi:10.1029/1999JD900923.
[51] Schuster GL, Dubovik O, Holben BN. Angstrom exponent and bimodal aerosol size distributions. J Geophys Res 2006;111(D7):D07207. doi:10.1029/2005JD006328.
[52] Smirnov A, Holben BN, Eck TF, Slutsker I, Chatenet B, Pinker RT. Diurnal variability of aerosol optical depth observed at AERONET (aerosol robotic network) sites. Geophys Res Lett 2002;29:28–31. doi:10.1029/2002GL016305.
[53] Kaufman YJ, Holben BN, Tanré D, Slutsker I, Smirnov A, Eck TF. Will aerosol measurements from Terra and Aqua polar orbitingsatellites represents the daily aerosol abundance and properties? Geophys Res Lett 2000;27:3861–4. doi:10.1029/2000GL011968.